JOURNAL OF SPACECRAFT AND ROCKETS
Vol. 41, No. 6, November–December 2004

Design of Tether Sling for Human Transportation Systems Between Earth and Mars

Michael D. Jokic*
University of Queensland, Brisbane, Queensland 4072, Australia
and
James M. Longuski†
Purdue University, West Lafayette, Indiana 47907-2023

Human transportation systems between Earth and Mars might benefit greatly from the construction of a tether sling facility on Phobos. A tether sling has the potential to launch vehicles from Phobos to Earth with little or no propellant expended because it is solar powered. For current trajectory designs and tether materials, we show that a tether sling facility is superior to chemical propulsion systems when multiple launches from Phobos are considered. A performance index of the ratio of tether mass to chemical-propellant mass is used to compare various mission scenarios. Ratios less than 10 are considered desirable. The most advantageous application of the tether sling occurs during a Hohmann transfer from Phobos to Earth where the mass ratio is 1.8. Next are semicyclers (ratios of 1.9 and 2.4) and a three-synodic-period cycler (8.7). Unfortunately, the Aldrin cycler does not benefit from the tether sling because the high hyperbolic velocity at Mars drives the mass ratio to infinity. For cases with desirable mass ratios, we also account for fluctuations in the cross section of the tether as a result of manufacturing uncertainties.

Nomenclature

A_x	=	cross-sectional area at location x along the tether sling, m^2
F_x	=	tensile force at location x along the tether sling, N
I_{sp}	=	specific impulse, s
l	=	tether length, m
m	=	mass, kg
m_p	=	payload mass, kg
m_t	=	tether mass, kg
V_∞	=	hyperbolic excess speed, m/s
v	=	velocity, m/s
v_c	=	material characteristic velocity, m/s
v^*	=	nondimensional velocity
Δ	=	variation in nominal cross-sectional area
ΔV	=	change in velocity, m/s
μ	=	planetary gravitational constant, m^3/s^2
ρ	=	tether material density, kg/m^3
σ	=	tether material tensile strength, Pa

Introduction

PUIG-SUARI et al.[1] propose a tether sling facility stationed at Phobos and show that once built it could provide an inexhaustible means of transporting vehicles and astronauts back to Earth. The sling is powered by solar-cell arrays to initiate and maintain spin rate. The basic elements of the tether sling concept are shown in Fig. 1. A payload connected to the hub by a long tether is spun up via torques applied at the hub. The payload is then launched onto a specified trajectory simply by being disconnected from the tether. For Hohmann transfers, the tether mass tends to be about the same as the propellant required in a chemical propulsion system. Kuchniki et al.[2] extend the work of Puig-Suari et al.[1] by examining the dynamics of a tether sling.

The mechanical advantages of tethers in space have been recognized for some time as reported in the handbook by Cosmo and Lorenzini.[3] An important benefit of tethered systems lies in their ability to be used for momentum transportation reducing, or eliminating, the need for expendable propellant. Indeed, there are several proposals demonstrating the potential of tethered systems to act as transport facilities.[4–7]

The efficiency of tether transportation facilities is strongly dependent on their constituent material properties and the shape of the tether. Tapered tether designs have been identified as important for ensuring mass efficiency and necessary to achieve designs capable of withstanding expected loads.[1,3,8,9] Recently, great strides have been made in increasing the ratio of material strength to weight. Tether concept designs employ a diverse range of materials that possess significantly better mechanical properties than metal cables.[1,10,11] The latest evolution of tether materials, including Spectra and Zylon,[6] have extremely high strength-to-weight ratios. Current research into carbon nanotubes[12] suggests incredible strength potential for materials in the future.

Research into cyclical, or cycler trajectories, began in the 1960s and continues to grow.[13–22] The aim is to establish practical transportation systems that require little maintenance while achieving reasonable arrival and departure velocities for the cycler vehicles.[23]

In this paper, we consider how advances in material science can open the door to a highly efficient tether sling facility stationed on Phobos. We assess the potential mass savings achieved via a tether sling facility for various human transportation systems between Earth and Mars.

Minimum-Mass Sling Designs

Tapered Tether Analysis

In a tether sling facility the maximum tension occurs at the attachment point between the tether and the hub. Conversely, the minimum tension occurs at the end of the tether where the payload mass is attached. Puig-Suari et al.[1] develop a tapered tether design that minimizes the mass of the tether by matching the cross-sectional area with the tension at a particular location along the tether. The following discussion outlines some of the key results from their analysis, which form the basis of the current tapered tether design.

Presented as Paper 2002-4642 at the AIAA/AAS Astrodynamics Specialists Conference, Monterey, CA, 5–8 August 2002; received 13 May 2003; revision received 25 September 2003; accepted for publication 29 September 2003.

*Ph.D. Candidate, Division of Mechanical Engineering; m.jokic@uq.edu.au. Member AIAA.

†Professor, School of Aeronautics and Astronautics, 315 N. Grant Street; longuski@ecn.purdue.edu. Associate Fellow AIAA.

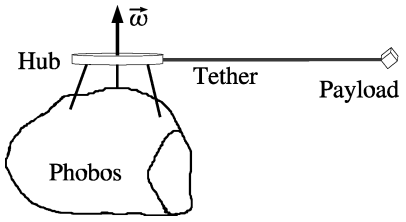

Fig. 1 Tether sling facility.

For a location along the tether at a distance x from the hub, the tensile force is

$$F_x = \int_x^l v^2 l^{-2} y \, \mathrm{d}m_y + v^2 l^{-2} m_p \tag{1}$$

The term $\mathrm{d}m_y$ is the mass of a differential tether element located at a distance y along the tether. For a maximum allowable acceleration and a given tip velocity, the length of the tether is determined using

$$l = v^2 / a_{\max} \tag{2}$$

From Eq. (1), the cross-sectional area of the tether at location x is represented as

$$A_x = F_x/\sigma = (v^2/\sigma l)\left[(\rho/l)\int_x^l y A_y \, \mathrm{d}y + m_p\right] \tag{3}$$

where A_y is the tether area at point y. By differentiating Eq. (3) and then integrating, the expression for the tether area becomes

$$A_x = A_l \exp[(\rho v^2/2\sigma)(1 - x^2 l^{-2})] \tag{4}$$

where A_l is the cross-sectional area of the tether at the end where the payload is attached:

$$A_l = m_p(v^2/\sigma l) \tag{5}$$

The mass of the tether is

$$m_t = \int_0^l \rho A_x \, \mathrm{d}x \tag{6}$$

By substituting for A_x and performing a change of variables, the tether mass can be expressed in terms of the error function as

$$m_t = m_p v(\rho/2\sigma)^{\frac{1}{2}} \pi^{\frac{1}{2}} \exp(\rho v^2/2\sigma) \operatorname{erf}\left[v(\rho/2\sigma)^{\frac{1}{2}}\right] \tag{7}$$

and in terms of a mass ratio as

$$m_t/m_p = \sqrt{\pi} v^* \exp(v^{*2}) \operatorname{erf}(v^*) \tag{8}$$

The nondimensional velocity v^* is calculated using

$$v^* = v\,(\rho/2\sigma)^{\frac{1}{2}} = v/v_c \tag{9}$$

Mission Scenarios

We assume that the tether sling is spun up gradually via torques generated by an electric motor at the hub. As discussed by Puig-Suari et al.,[1] the power needed to spin the sling can be provided by solar-cell arrays. A likely location for the tether sling facility is at the north pole of Phobos to avoid collision between the sling and the surface of Phobos. Thus the spin plane of the sling is predominantly in the orbital plane of Phobos with some plane variation possible by articulation of the hub. Significant plane change would necessarily require propulsive maneuvers. However, these maneuvers would be small compared to the in-plane velocity achieved by the tether sling.

In sizing the tether sling facility, we divide potential mission scenarios into two categories: 1) those involving stopovers and 2) pure cyclers. The first category includes semicyclers, Hohmann transfers, rapid transfers (with time of flight less than half a year), and Mars free returns. In each case, the vehicle being launched from Phobos is assumed to have a mass of 70 Mg (metric tons). For comparison, the mass needed to achieve the same launch conditions for a single-stage chemical rocket employing liquid oxygen and methane (LOX/CH_4) is computed. The ratio of the structural mass to the propellant mass is assumed to be 0.15.

Table 1 Tether material mechanical properties

Property	Spectra 2000	Zylon	Kevlar	Hercules IM7
Tensile strength, GPa	3.50	5.80	2.80	4.82
Density, kg/m^3	970	1560	1450	1550

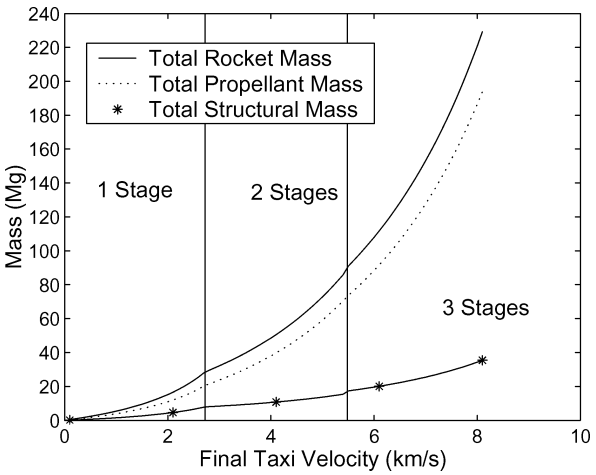

Fig. 2 Mass profile of the taxi rocket model.

The second category considers pure cyclers where the tether sling launches taxi vehicles onto a rendezvous trajectory with a cycler vehicle as the cycler flies by Mars. In this scenario, the taxi mass is about 11 Mg. Unlike the stopover vehicles, the taxi does not need to carry the life-support mass needed to sustain astronauts for the flight to Earth. Hence, the taxi vehicle has significantly less mass than the stopover vehicle. Two rocket models, which use LOX/CH_4 propellant, are included in the cycler category for comparison. The first model assumes a single-stage rocket, whereas the second model consists of multiple stages to closely match the Mars taxi system proposed by Nock.[20] Figure 2 shows the propellant mass performance profile of the Mars taxi model used in the current investigation.

Tether Sling Performance

The performance of the tether sling, in terms of mass, is dependent on the mechanical properties of the tether material. Table 1 lists the mechanical properties for several tether materials described in the literature. To determine the performance of the tether sling, we compare the mass of the tether to the mass of the propellant required to meet the launch needs of a specified mission scenario. Because of the reusability of the tether sling, we assume that tether-mass-to-propellant-mass ratios of up to 10 are acceptable. The tether-mass-to-propellant-mass ratio indicates the number of launches required for the tether mass to match the propellant mass needed for the launches. Any launches in excess of the value of tether-mass-to-propellant-mass ratio represent a significant mass saving.

Figure 3 presents the tether-mass-to-propellant-mass ratios for launching a taxi vehicle with a single-stage rocket model. Clearly, the materials with high strength-to-weight ratios produce more favorable mass ratios. This is particularly evident at higher launch velocities. The 2010 material is a hypothetical product of the future assumed to possess a strength-to-weight ratio about 1.5 times that of Spectra 2000. We note that the strength-to-weight ratios of the Spectra 2000 and Zylon materials are similar, resulting in closely matching mass-performance profiles. Similar trends are observed in

Table 2 Potential trajectories for human transportation systems between Earth and Mars

Trajectory	Description	Trajectory category	Characteristic hyperbolic excess speed, V_∞, km/s	Source
Semicycler 1, 2018	Mars launch (in 2018) and arrival with two Earth flybys	1) Stopover	2.76	Aldrin et al.[22]
Semicycler 2, 2018	Mars launch (in 2018) and arrival with three Earth flybys	1) Stopover	3.27	Aldrin et al.[22]
M-E Hohmann	Mars to Earth Hohmann transfer	1) Stopover	2.64	Puig-Suari et al.[1]
M-E (<1/2 yr)	Mars to Earth with a time of flight less than half a year	1) Stopover	3.00	STOUR[24] search
M-E-M	Mars launch and arrival with a single flyby of Earth	1) Stopover	4.00	STOUR[24] search
Repeating sequence of M-E-E-E-M	Cycler trajectory repeating every three synodic periods	2) Pure cycler	5.47	Chen et al.[23]
Aldrin cycler	Cycler trajectory repeating every two synodic periods	2) Pure cycler	11.9	Chen et al.[25]

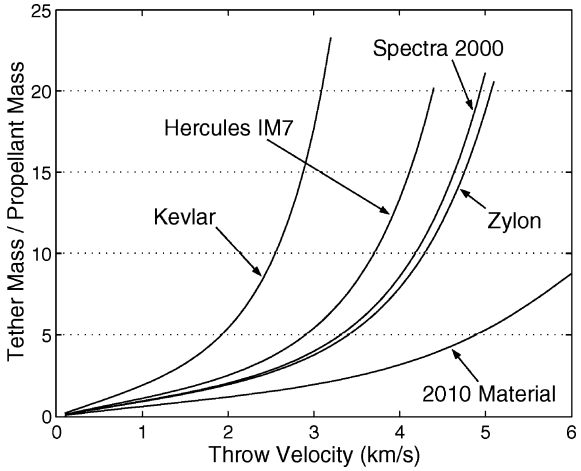

Fig. 3 Tether-mass-to-propellant-mass ratio vs throw velocity for a taxi vehicle launch (single-stage rocket model).

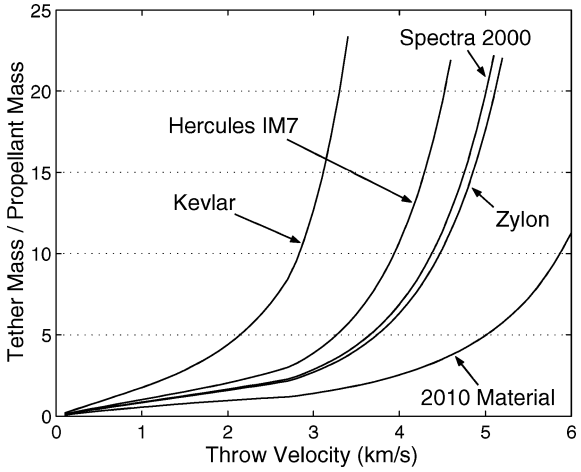

Fig. 4 Tether-mass-to-propellant-mass ratio vs throw velocity for a taxi vehicle launch (taxi rocket model).

Fig. 4, which represents the mass performance of the tether sling relative to the propellant requirements calculated with the Mars taxi model. Comparing Fig. 4 to Fig. 3, we see that the lower propellant needs of the multistage rocket produce higher tether-mass-to-propellant-mass ratios than for the single-stage rocket model at high launch velocities (>5.3 km/s). We note that the curves in Fig. 3 are unaffected by replacing the payload with a stopover vehicle. (By changing from a taxi vehicle to a stopover vehicle the payload mass, propellant mass, and tether mass all increase by a factor of 6.3.)

The transfer trajectories forming the basis of our tether designs are summarized in Table 2. As the table indicates, we develop tether sling designs for five stopover trajectories and two cycler trajectories. Each mission scenario requires the sling to produce a different velocity at the tip to accommodate the hyperbolic excess speeds of the trajectories at Mars. We assume that the tether sling launches a large vehicle of 70 Mg to transfer astronauts and cargo from Phobos to Earth via the stopover trajectories. The stopover trajectory scenarios require the vehicle to travel between Mars and Earth with stays at Mars and/or Earth. In the cycler trajectory scenarios the tether sling launches a smaller vehicle of 11 Mg to transfer astronauts and cargo to a large vehicle in the vicinity of Mars. We assume that the large destination vehicle is in a trajectory with periodic flybys of Mars and Earth.

First among the stopover scenarios are two versions of semicycler trajectories proposed by Aldrin et al.[22] The semicycler trajectories involve launches and arrivals at Mars with multiple flybys of Earth. In our analysis, we develop tether designs for launches in 2018. The next trajectory is a direct Mars-to-Earth (M-E) transfer corresponding to the minimum-energy Hohmann transfer. Approximate values of the hyperbolic excess speeds needed to achieve the last two stopover trajectories (for several launch years) are obtained from the Satellite Tour Design Program (STOUR),[24] a patched-conic propagator. The last stopover scenarios correspond to an M-E transfer (with time of flight less than half a year) and a trajectory involving launches and arrivals at Mars with single gravity-assist flybys of Earth.

The final trajectories[23,25,26] presented in Table 2 belong to our second trajectory category where the tether sling launches a taxi vehicle to rendezvous with a vehicle in a cycler orbit. The Aldrin cycler consists of two cycler vehicles called an up-cycler and a down-cycler. The up-cycler is in an elliptic orbit about the sun such that it has a type 1 transfer from Earth to Mars every synodic period (2.14 years). (A type 1 transfer is an arc that is less than half an elliptic orbit about the sun.) Conversely, the down-cycler has a type 1 transfer from Mars to Earth every synodic period. Our final cycler trajectory is a patched semicycler consisting of connected sequences of M-E-E-E-M flybys.[23] The cycler repeats in the heliocentric frame every three synodic periods.

We see in Table 3 that the tether sling compares favorably to the rocket in terms of mass for the stopover trajectories. The mechanical properties of Zylon are adopted for the sling designs. We assume that the tether sling imparts enough change in velocity to provide the payload with the hyperbolic excess speed required for each mission scenario. The largest tether-mass-to-propellant-mass ratio is 3.5 for the first trajectory category. Because the tether sling is a reusable system, significant mass savings will be achieved via the tether sling after the fourth launch. The tether lengths for the stopover scenarios range from 120 to 281 km with a corresponding diameter range at

Table 3 Tether sling system properties for transfer trajectories between Earth and Mars

System parameter	Semi-cycler 1 2018	Semi-cycler 2 2018	M-E Hohmann	M-E (<1/2 yr)	M-E-M	Repeating sequence of M-E-E-E-M	Aldrin cycler
Payload mass, Mg	70.0	70.0	70.0	70.0	70.0	11.2	11.2
V_∞, km/s	2.76	3.27	2.64	3.00	4.00	5.47	11.9
ΔV, km/s	1.96	2.32	1.88	2.12	2.88	4.11	10.18
Max. acceleration, g	3.00	3.00	3.00	3.00	3.00	3.00	3.00
I_{sp}, s	379	379	379	379	379	379	379
Single-stage prop., Mg	54.1	69.5	51.0	60.9	99.1	32.5	Invalid
Taxi model prop., Mg	——	——	——	——	——	39.9	483
Length, km	130	182	120	153	281	575	3520
Diameter at end, cm	2.13	2.13	2.13	2.13	2.13	0.850	0.850
Diameter at hub, cm	2.75	3.05	2.69	2.88	3.71	2.65	897
Tether mass, Mg	103	166	92	129	344	281	8.25×10^7
μ_{single}[a]	1.90	2.40	1.80	2.12	3.47	8.65	Invalid
μ_{taxi}[b]	——	——	——	——	——	7.03	1.71×10^5

[a] μ_{single} = tether mass to single-stage propellant mass ratio. [b] μ_{taxi} = tether mass to taxi model propellant mass ratio.

the hub of 2.69 to 3.71 cm. The tether lengths are a consequence of the tip velocity and our assumed 3-g acceleration limit [Eq. (2)]. Clearly, the most favorable result is the M-E Hohmann transfer with a tether-mass-to-propellant-mass ratio of only 1.80. In this scenario, significant mass savings will be achieved after two launches.

The size of the tether needed for the Aldrin cycler is prohibitively large because the hyperbolic excess speed at Mars can reach 11.9 km/s. There is no propellant mass listed under the Aldrin cycler corresponding to the single-stage rocket model as the required velocity change cannot be achieved with the specified I_{sp} of 379 s. For the other cycler trajectory, however, the tether sling performance is extremely encouraging. The mass ratio for the patched semicycler trajectory is less than 9, which is reasonable, allowing for the reusability of the tether system.

We can see from Table 3 that the tether diameter at the end is dependent on the size of the payload. For the stopover trajectories with a payload of 70 Mg, the diameter at the end of the tether is 2.13 cm. The diameter at the end of the sling is only 0.85 cm for the taxi payload. Except for the M-E-M trajectory, the mass of the tether sling for the stopover scenarios is less than the cycler trajectories. The more massive payload of the M-E-M trajectory results in a tether design with a larger mass than the patched semicycler scenario. The difference between the masses is not an obvious result, as the cycler requires a greater throw velocity and a longer tether.

The tether designs outlined here represent the minimum-mass configurations of the tether sling needed to perform the various mission scenarios. Although the trends are extremely encouraging, other considerations are necessary for practical tether sling designs.

Practical Sling Designs

The minimum-mass design does not allow for errors in the manufacture of the tether, which can result in fluctuations in the cross-sectional area along the length of the tether. In the following analysis we assess the mass cost of compensating for manufacturing errors. We do not include a safety factor in our analysis.

The cross-sectional area of the tapered tether can take several profiles depending upon whether a cable or tape tether is adopted. A tape tether has a flattened cross section. It is roughly a plane figure, which is thin (and of constant thickness) in the out-of-plane direction and tapered in one dimension. Cable tethers have circular cross sections. To keep the analysis of the effect of manufacturing errors general, we consider fluctuations in cross-sectional area as opposed to dimensional tolerances.

To withstand errors in cross-sectional area in the worst case, the minimum area at a particular location along the tether must be capable of supporting the tensile forces generated by the tether possessing maximum area at all other locations. By this principle, the area at the end of the tether calculated by the minimum-mass analysis becomes the minimum allowable area at that location. The minimum

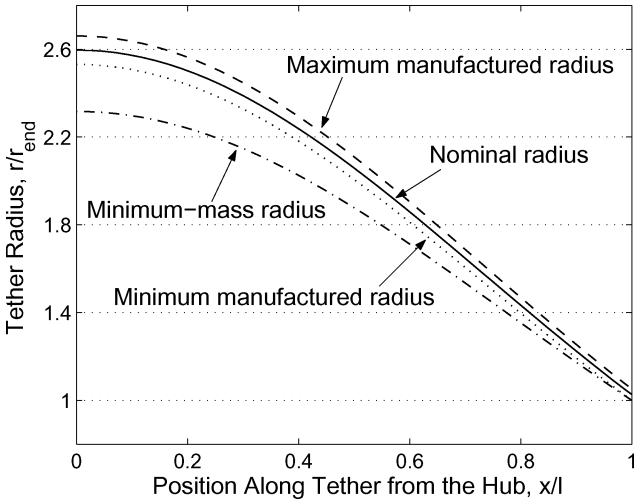

Fig. 5 Nondimensional tether radius vs nondimensional position along the tether.

tip area relates to the nominal design area by

$$A_{l\,\min} = m_p(v^2/\sigma l) = (1-\Delta)A_{l\,\text{nom}} \tag{10}$$

This is assuming that any nominal cross-sectional area can fluctuate by a factor of $1 \pm \Delta$. Subsequently, the maximum possible area at the tether tip is

$$A_{l\,\max} = (1+\Delta)(1-\Delta)^{-1}A_{l\,\min} \tag{11}$$

Following the minimum-mass analysis, the maximum possible cross-sectional area at any location along the tether is

$$A_{x\,\max} = A_l \exp[(1+\Delta)(1-\Delta)^{-1}(v^2\rho/2\sigma)(1-x^2l^{-2})] \tag{12}$$

The corresponding maximum tether mass is defined as

$$m_{t\,\max} = A_l \exp[(1+\Delta/1-\Delta)(v^2\rho/2\sigma)] \times \int_0^l \exp[-(1+\Delta/1-\Delta)(v^2\rho/2\sigma)x^2l^{-2}]\,\mathrm{d}x \tag{13}$$

Again using a change of variables, the mass ratio is

$$m_{t\,\max}/m_p = \pi^{\frac{1}{2}}v^*(1-\Delta/1+\Delta)^{\frac{1}{2}} \times \exp[v^{*2}(1+\Delta/1-\Delta)]\,\mathrm{erf}\left[v^*(1+\Delta/1-\Delta)^{\frac{1}{2}}\right] \tag{14}$$

The implications of the potential fluctuations in cross-sectional area to the mass of the tether become evident by examining Fig. 5.

Table 4 Tether sling system properties for transfer trajectories between Earth and Mars allowing for fluctuations in the cross-sectional area of the tether

System parameter	Semi-cycler 1 2018	Semi-cycler 2 2018	M-E Hohmann	M-E (<1/2 yr)	M-E-M	Repeating sequence of M-E-E-E-M	Aldrin cycler
Payload mass, Mg	70.0	70.0	70.0	70.0	70.0	11.2	11.2
V_∞, km/s	2.76	3.27	2.64	3.00	4.00	5.47	11.9
ΔV, km/s	1.96	2.32	1.88	2.12	2.88	4.11	10.2
Length, km	130	182	120	153	281	575	3520
Fluct. Fact., Δ	0.05	0.05	0.05	0.05	0.05	0.05	0.05
Max. diameter at end, cm	2.24	2.24	2.24	2.24	2.24	0.89	0.89
Nom. diameter at end, cm	2.13	2.13	2.13	2.13	2.13	0.85	0.85
Min. diameter at end, cm	2.02	2.02	2.02	2.02	2.02	0.81	0.81
Max. diameter at hub, cm	2.97	3.33	2.90	3.12	4.13	3.14	1960
Nom. diameter at hub, cm	2.83	3.17	2.77	2.97	3.94	2.99	1870
Min. diameter at hub, cm	2.69	3.01	2.63	2.83	3.74	2.84	1780
Max. tether mass, Mg	107	176	95	135	376	342	3.40×10^8
Max. μ_{single}[a]	1.97	2.54	1.86	2.21	3.79	10.5	Invalid
Max. μ_{taxi}[b]	——	——	——	——	——	8.57	7.03×10^5

[a] μ_{single} = tether mass to single-stage propellant mass ratio. [b] μ_{taxi} = tether mass to taxi model propellant mass ratio.

The figure represents nondimensionally the radius of the tether at each location along a cable tether sling for both the practical and minimum-mass designs. As expected, the radius for the design including fluctuations in area is greater at nearly all locations than the minimum-mass design. The only overlap between the designs occurs at the tether tip, where the minimum manufactured radius is equal to the minimum-mass value. The difference between the tether radius produced from the minimum-mass and practical design techniques is dependent on the area fluctuation factor Δ. For the results depicted in Fig. 5, a value of 0.05 is used for the fluctuation factor.

The inclusion of fluctuations in the cross-sectional area alters the minimum-mass results obtained for the transfer trajectories between Earth and Mars. Table 4 contains modified results from those presented in Table 3 for the minimum-mass analysis. The details of the trajectories and the corresponding propellant requirements are unchanged. However, the physical dimensions and mass of the tether have increased. For each of the trajectories listed, three diameters are included for the tether tip and hub attachment point. These values correspond to the maximum, minimum, and nominal manufactured diameters of the tether. For the purposes of discussing the worst tether-sling-mass performance, the maximum tether mass and mass ratio results are included. In general, however, the mass of the tether will tend toward the most likely configuration, which is the nominal tether design.

We see in Table 4 that the range of tether lengths is the same as for the cases presented in Table 3. The dependence of the diameter at the end of the sling on the payload mass is again abundantly clear. In all of the five stopover mission scenarios, the manufactured diameter at the end of the sling ranges from 2.02 to 2.24 cm. For the pure cycler trajectories, the diameter at the end of the sling ranges from 0.81 to 0.89 cm. The diameter ranges at the hub for stopover trajectories corresponding to the maximum, nominal, and minimum cases are 1.23, 1.17, and 1.11 cm, respectively. In all cases, the ranges for the stopover trajectories are greater than the 1.02-cm-diam range of the minimum-mass design. The maximum masses reported in Table 4 are larger than the minimum-mass values of Table 3. For the practical design corresponding to the Hohmann transfer, the maximum possible increase in mass relative to the minimum-mass design is only 3 Mg. The patched semicycler, however, shows a potential mass increase of 61 Mg.

For the scenarios with lower throw velocities, the effect of the adjusted tether design on the tether-mass-to-propellant-mass ratio is quite small. In most cases, the mass ratio continues to remain under 10. The exceptions to this are the Aldrin cycler and the M-E-E-E-M patched semicycler trajectories. For the patched semicycler, the mass ratio corresponding to the single-stage-rocket model has increased from 8.65 to 10.5. With a maximum mass ratio of 3.79 for the M-E-M trajectory, the stopover scenarios still benefit from a tether sling with the least number of launches.

Incorporating a safety factor into the design will further increase the tether masses and, subsequently, the mass ratios reported in Table 4. For the development of an effective tether sling, or any mass-sensitive tether application, nonideal designs must be considered. The limitations of the manufacturing processes and accounting for uncertainties through the inclusion of an appropriate safety factor are crucial issues in practice.

Conclusions

Multiple launches via a tether sling stationed on Phobos can result in enormous mass savings for a human transportation system between Earth and Mars. We have shown that the tether sling is particularly beneficial to stopover trajectories as all of the tether-mass-to-propellant-mass ratios are less than four for the mission scenarios presented. Our investigation has revealed that the Mars flyby conditions of the Aldrin cycler cannot be accommodated with a tether sling. However, a transportation system employing a cycler trajectory with repeating sequences of M-E-E-E-M flybys will gain enormous mass savings via a tether sling after nine launches. Our final sling designs employ a strategy to accommodate fluctuations in the cross-sectional area of the tether caused by manufacturing errors. Allowing for uncertainties in the fabrication of a tether is important for any mass-sensitive tether application. With continued advancements in the field of material science and improvements in trajectory designs, the mass performance of a tether sling facility will greatly improve. Ultimately, a tether sling facility on Phobos might be of tremendous benefit to advancing human exploration of space.

Acknowledgment

This work was made possible, in part, through the Graduate School Research Travel Award of the University of Queensland's Graduate School.

References

[1]Puig-Suari, J., Longuski, J. M., and Tragesser, S. G., "A Tether Sling for Lunar and Interplanetary Exploration," *Acta Astronautica*, Vol. 36, No. 6, 1995, pp. 291–295.

[2]Kuchnicki, S. N., Tragesser, S. G., and Longuski, J. M., "Dynamics of a Tether Sling," American Astronautical Society, Paper 97-605, Aug. 1997.

[3]Cosmo, M. L., and Lorenzini, E. C. (eds.), *Tethers in Space Handbook*, 3rd ed., Smithsonian Astrophysical Observatory, Cambridge, MA, 1997.

[4]Hoyt, R. P., and Uphoff, C. W., "Cislunar Tether Transport System," *Journal of Spacecraft and Rockets*, Vol. 37, No. 2, 2000, pp. 177–186.

[5]Nordley, G., and Forward, R., "Mars–Earth Rapid Interplanetary Tether Transport System: Initial Feasibility Study," *Journal of Propulsion and Power*, Vol. 17, No. 3, 2001, pp. 499–507.

[6]Bogar, T. J., Bangham, M. E., Forward, R. L., and Lewis, M. J., "Hypersonic Airplane Space Tether Orbital Launch (HASTOL) System: Interim Study Results," AIAA Paper 99-4802, Nov. 1999.

[7]Colombo, G., "The Use of Tether for Payload Orbit Transfer," NASA Rept. N82-26705, March 1982.

[8]Tillotson, B., "Tether as Upper Stage for Launch to Orbit," AIAA Paper 89-1585, May 1989.

[9]Arnold, D. A., "The Behavior of Long Tethers in Space," *Journal of the Astronautical Sciences*, Vol. 35, No. 1, 1987, pp. 3–18.

[10]Pasca, M., and Lorenzini, E. C., "Collection of Martian Atmospheric Dust with a Low Altitude Tethered Probe," *Advances in the Astronautical Sciences*, Vol. 75, Feb. 1991, pp. 1121–1139.

[11]Pasca, M., and Lorenzini, E. C., "Optimization of a Low Altitude Tethered Probe for Martian Atmospheric Dust Collection," *Journal of the Astronautical Sciences*, Vol. 44, No. 2, 1996, pp. 191–205.

[12]Smitherman, D. V., Jr., "Space Elevators: An Advanced Earth-Space Infrastructure for the New Millennium," NASA CP-2000-210429, Aug. 2000.

[13]Hollister, W. M., "Castles in Space," *Astronautica Acta*, Vol. 14, No. 2, 1969, pp. 311–316.

[14]Rall, C. S., and Hollister, W. M., "Free-Fall Periodic Orbits Connecting Earth and Mars," AIAA Paper 71-92, Jan. 1971.

[15]Friedlander, A. L., Niehoff, J. C., Byrnes, D. V., and Longuski, J. M., "Circulating Transportation Orbits Between Earth and Mars," AIAA Paper 86-2009, Aug. 1986.

[16]Aldrin, B., "Cyclic Trajectory Concepts," SAIC Presentation to the Interplanetary Rapid Transit Study Meeting, Jet Propulsion Lab., Pasadena, CA, Oct. 1985.

[17]Byrnes, D. V., Longuski, J. M., and Aldrin, B., "Cycler Orbit Between Earth and Mars," *Journal of Spacecraft and Rockets*, Vol. 30, No. 3, 1993, pp. 334–336.

[18]Hoffman, S. J., Friedlander, A. L., and Nock, K. T., "Transportation Node Performance Comparison for a Sustained Manned Mars Base," AIAA Paper 86-2016, Aug. 1986.

[19]Bishop, R. H., Byrnes, D. V., Newman, D. J., Carr, C. E., and Aldrin, B., "Earth-Mars Transportation Opportunities: Promising Options for Interplanetary Transportation," American Astronautical Society, Paper 00-255, March 2000.

[20]Nock, K. T., "Cyclical Visits to Mars via Astronaut Hotels," NASA Inst. for Advanced Concepts, Univs. Space Research Association, Phase I Final Rept., Research Grant 07600-049, 30 Nov. 2000.

[21]Nock, K. T., and Friedlander, A. L., "Elements of a Mars Transportation System," *Acta Astronautica*, Vol. 15, No. 6/7, 1987, pp. 505–522.

[22]Aldrin, B., Byrnes, D., Jones, R., and Davis, H., "Evolutionary Space Transportation Plan for Mars Cycling Concepts," AIAA Paper 2001-4677, Aug. 2001.

[23]Chen, K. J., Landau, D. F., McConaghy, T. T., Okutsu, M., Longuski, J. M., and Aldrin, B., "Trajectory Analysis and Design of Mars Cyclers: Preliminary Assessment," AIAA Paper 2002-4422, Aug. 2001.

[24]Rinderle, E. A., "Galileo User's Guide, Mission Design Systems, Satellite Tour Analysis and Design Subsystem," Jet Propulsion Lab., JPL D-263, California Inst. of Technology, Pasadena, CA, July 1986.

[25]Chen, K. J., McConaghy, T. T., Okutsu, M., and Longuski, J. M., "A Low-Thrust Version of the Aldrin Cycler," AIAA Paper 2002-4421, Aug. 2002.

[26]McConaghy, T. T., Longuski, J. M., and Byrnes, D. V., "Analysis of a Class of Earth–Mars Cycler Trajectories," *Journal of Spacecraft and Rockets*, Vol. 41, No. 4, 2004, pp. 622–628.

C. Kluever
Associate Editor